Vol. 6 • No. 13 • July 6 • 2016
www.advenergymat.de

ADVANCED ENERGY MATERIALS

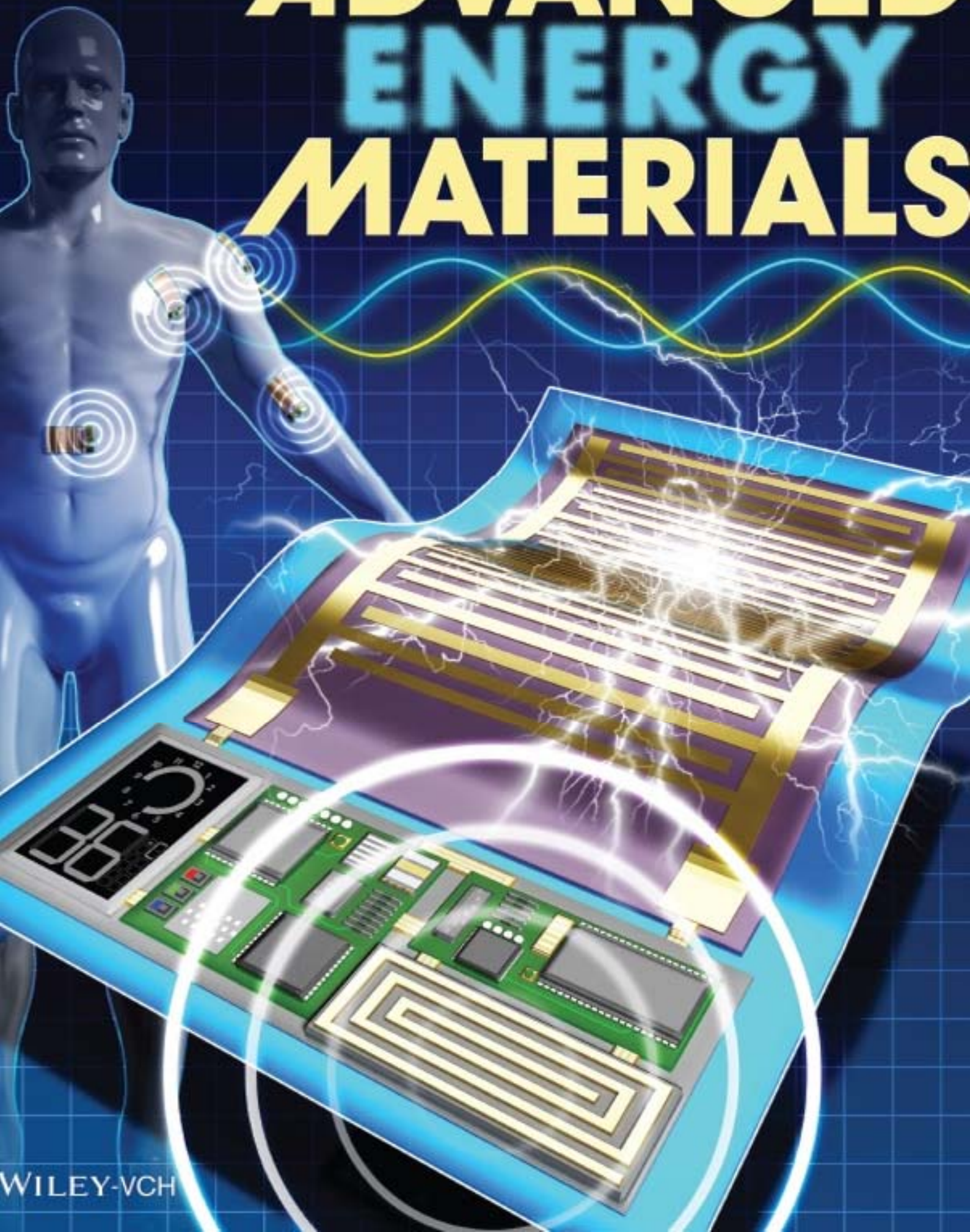

WILEY-VCH

Self-Powered Wireless Sensor Node Enabled by an Aerosol-Deposited PZT Flexible Energy Harvester

Geon-Tae Hwang, Venkateswarlu Annapureddy, Jae Hyun Han, Daniel J. Joe, Changyeon Baek, Dae Yong Park, Dong Hyun Kim, Jung Hwan Park, Chang Kyu Jeong, Kwi-Il Park, Jong-Jin Choi, Do Kyung Kim, Jungho Ryu, and Keon Jae Lee**

In the coming era of internet of things (IoT), the wireless sensor network (WSN) is a key technology to analyze and control all information related to public safety, human healthcare, industrial automation, and environmental monitoring.[1] To operate a WSN, bulky batteries are widely used as the power source, and inevitably these batteries should be periodically replaced due to their limited capacity.[2] However, the battery maintenance of a million sensor nodes would be practically impossible from the perspective of human effort and expenses, which is the biggest obstacle to the wide commercialization of the IoT.[3] In this regard, self-powered energy-harvesting systems for the individual sensor nodes should be developed for maintenance-free, sustainable, and independent operation of extensive WSN applications.[4]

Flexible piezoelectric energy harvesters, called nanogenerators (NGs), have been studied by many research groups as they can harvest electrical power from ambient mechanical and vibrational energy such as structure/motor vibration, gentle airflow, and even tiny biomechanical movements of muscles/organs.[5–10] Many piezoelectric materials, such as ZnO, $BaTiO_3$, and $Pb(Zr_x,Ti_{1-x})O_3$ (PZT), were utilized to realize flexible piezoelectric-harvesting devices for self-powered electronics.[11–17] For example, a self-powered wireless sensor node was constructed using a ZnO NG as a power source for a photodetecting sensor.[18] Nevertheless, the relatively low output performance (generated voltage and current of 10 V and 1.4 μA, respectively) of the ZnO device should be improved to realize practical WSN applications. To address this issue, our group recently developed high-performance flexible energy harvesters by using single-crystalline piezoelectric materials with a high piezoelectric d_{33} constant of above 2000 pC N^{-1}.[19–21] Although these energy harvesters provided instantaneous milli-Watt-level peak power to operate various electronic and biomedical devices, the high production cost of single crystals could impede the commercialization of flexible piezoelectric energy harvesters.[22,23] The conventional sol-gel coating technique for dense piezoelectric films with a thickness of a few micrometers is also not favorable for industrial application due to the multiple tedious repetitions of both spin coating and heat treatment of each 100-nm layer to minimize film cracking caused by excessive tensile stress during the annealing process.[24]

Aerosol deposition (AD), proposed by Akedo and Lebedev, can provide fast, thick, and cost-effective deposition of high-quality piezoelectric films:[25] This unique AD process can instantaneously produce nanograined polycrystalline ceramic thick films that are up to several hundred micrometers in thickness, and which have similar piezoelectric properties to those of bulk ceramics on various substrates (e.g., silicon, sapphire, quartz, and metals) without cracking.[26,27] To facilitate high-kinetic-energy bombardment of ceramic particles, micrometer-sized piezoelectric granules are accelerated to a nearly sonic speed (up to 300 m s^{-1}) to collide with the target substrates at room temperature, followed by subsequent high-temperature grain growth to improve the piezoelectric properties of the AD films.[28] While application of AD ceramic films in piezoelectric fields such as microelectromechanical systems (MEMS) generators, actuators, and ultrasonic transducers was studied, AD films were not widely exploited for flexible applications due to their intrinsic brittleness and rigidity.[26]

Here, we demonstrate a high-performance flexible piezoelectric energy harvester enabled by an AD-based PZT thick film on a plastic substrate to develop a self-powered wireless sensor-node system. A high-temperature (900 °C) annealed crystalline AD PZT film with a thickness of 7 μm on a rigid sapphire substrate was successfully transferred onto a flexible substrate by an inorganic-based laser lift-off (ILLO) without any structural damage or degradation of its properties.[29] Our flexible PZT harvesting device can generate an open-circuit voltage of 200 V and a short-circuit current of 35 μA by biomechanical bending/unbending motions. The high-output performance of the AD PZT harvester is comparable with the performance of a previous flexible single-crystal piezoelectric harvester, which is attributed to the high-temperature grain growth of AD films.[20] The harvested electricity was used to directly light up 208 blue

Dr. G.-T. Hwang, J. H. Han, Dr. D. J. Joe, C. Baek, D. Y. Park, D. H. Kim, J. H. Park, Dr. C. K. Jeong, Prof. D. K. Kim, Prof. K. J. Lee
Department of Materials Science and Engineering
Korea Advanced Institute of Science and Technology (KAIST)
291 Daehak-ro, Yuseong-gu
Daejeon 34141, Republic of Korea
E-mail: keonlee@kaist.ac.kr

Dr. V. Annapureddy, Dr. J.-J. Choi, Dr. J. Ryu
Functional Ceramics Group
Korea Institute of Materials Science (KIMS)
797 Changwondaero
Seongsan-gu, Changwon, Gyeongnam 51508, Republic of Korea
E-mail: jhryu@kims.re.kr

Prof. K.-I. Park
Department of Energy Engineering
Gyeongnam National University of Science and Technology (GNTech)
33, Dongjin-ro, Jinju, Gyeongsangnam-do 52725, Republic of Korea

DOI: 10.1002/aenm.201600237

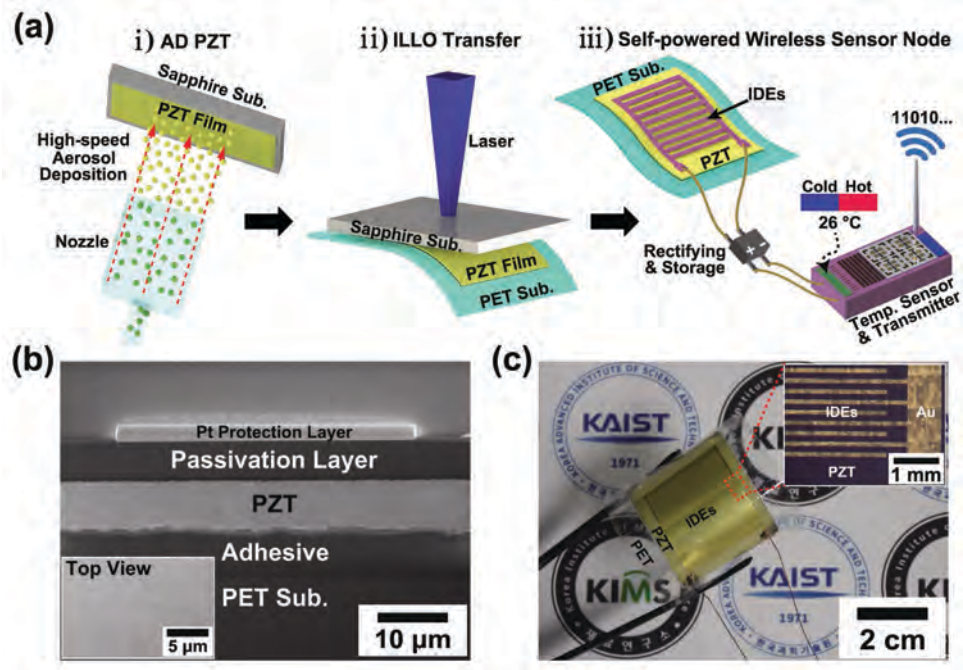

Figure 1. a) Schematic illustration of the device-fabrication process and self-powered WSN using a flexible AD PZT energy harvester enabled by ILLO. b) A cross-sectional SEM image of the AD PZT thick film on a PET substrate. The inset shows a top-view SEM image of the flexible PZT thick film. c) An optical image of the flexible PZT harvester bent by tweezers. The inset shows a top-view OM image of metal IDEs on the PZT.

LEDs and charge a supercapacitor. Finally, a self-powered wireless temperature sensor node was built by integrating the AD PZT energy harvester, rectifying/storage elements, a temperature-sensing processor, and a wireless radiofrequency (RF) transmitter. During the rectifying and storing stage, the alternating current (AC) output of the flexible harvester was converted into a direct current (DC) signal to charge a 1 mF capacitor up to 4.3 V within about 45 min. The stored self-powered energy was used to measure ambient temperature and then successfully transmit the RF data 18 times to a transceiver.

Figure 1a schematically shows the device-fabrication process and self-powered sensor-node application. The following explains the process in detail: i) The PZT film (thickness of 7 μm) is formed by AD process on a sapphire substrate at room temperature by using commercially available PZT granules (average granule size of ca. 100 μm, particle size of ca. 1.5 μm, see Table S1 in the Supporting Information for electromechanical properties). The PZT thickness of 7 μm was selected to balance piezoelectric output performance and film flexibility; the generated electric power is proportional to the thickness of the piezoelectric film while the film flexibility is inversely proportional to the film thickness.[30–33] This PZT material has high piezoelectric constants, d_{33} up to 406 pC N^{-1} and g_{33} up to 49.5 mV m N^{-1}, which are suitable for a high-performance piezoelectric energy harvester. The PZT particles mingle with the carrier gas in a granule feeding chamber, and then the accelerated granules are ejected under a vacuum from the spray nozzle to be bombarded onto the sapphire wafer with high speed at room temperature.[28] Subsequently, the AD PZT film is annealed at different temperatures (700–900 °C) for 1 h in a furnace to improve the piezoelectric and ferroelectric properties; the evaporation of PbO from the mother PZT could occur above 900 °C, which severely degrades the material properties of PZT.[34,35] ii) The PZT film (area of 3 × 4 cm^2) on the sapphire wafer is bonded onto a polyethylene terephthalate (PET) substrate (125 μm in thickness) by using an ultraviolet (UV)-sensitive polyurethane (PU) adhesive, and then the PU is optically cured by using UV light to attach the PZT film onto the flexible substrate. The thickness of plastic substrate was also selected to consider the electric output and flexibility of piezoelectric harvester; at a specific bending radius, a thick substrate enables us to derive higher output signals from the PZT than a thin substrate, due to a large induced strain on the piezoelectric film, whereas the thick substrate could cause deficient flexibility of device due to a high bending stiffness of the thick plastic layer.[30] To remove the sacrificial sapphire wafer from the AD PZT film, an XeCl excimer laser (wavelength of 308 nm) is used to irradiate the backside of the sapphire wafer using ILLO.[36] The laser beam (photon energy of 4.03 eV) can pass through the sapphire substrate (band gap energy of 10 eV) and is absorbed onto the surface of the PZT material (band gap energy of 3.3 eV) to induce local vaporization in the interface between the PZT ceramic and sapphire layer, which thereby separates the AD PZT film on the flexible substrate from the mother sapphire substrate.[37] This ILLO process enables stable, simple, and large-area transfer of high-quality inorganic films annealed at high temperature onto plastic substrates.[38] iii) Au interdigitated electrodes (IDEs) and an epoxy passivation layer are formed on the flexible PZT film. The photocurable PU protection layer can provide mechanical and electrical instability of the device during the poling and energy-harvesting processes.[36] Lastly, two Cu wires are linked to the metal pads, and then a poling process (applying electric field of 7 kV mm^{-1}) is performed to align internal dipoles of the flexible PZT film

at temperature of 70 °C for 3 h, which maximizes the piezoelectric properties of the PZT material for the high-output performance of our flexible energy harvester.[31] The finished flexible energy-harvesting device can generate electric power using a small or even slight movement compared to its initial state of PZT on a rigid sapphire wafer, since the bending stiffness of flexible piezoelectric harvester is much smaller than that of the AD PZT on the mother sapphire substrate (see Figure S1 in Supporting Information).

Figure 1b shows a cross-sectional scanning electron microscopy (SEM) image of the AD PZT thick film on a PET substrate after the ILLO process. A focused ion beam (FIB) was utilized as a milling cutter to prepare the cross-sectional surface. The 7 µm PZT film attached to the adhesive PU layer without mechanical damage, such as cracks or blisters in the ceramic layer, as compared to before ILLO transfer (see Figure S2 in Supporting Information). Figure 1c presents a photograph of a final flexible PZT harvester bent by tweezers, and the inset shows a magnified optical microscopy (OM) image of lateral-type IDEs on the flexible piezoelectric film. The IDEs had a total area of 2.5×3 cm^2, finger length of 2.4 cm, an electrode width of 90 µm, an electrode interdistance of 100 µm, and 70 finger pairs.

The output performance of flexible piezoelectric energy harvesters can be greatly enhanced by increasing grain size as a function of annealing temperature.[39] We annealed the AD PZT thick films on sapphire substrates at different temperatures of 700, 800, and 900 °C in a furnace for 1 h, and investigated the structural and ferroelectric properties of the samples by using SEM, X-ray diffraction (XRD), the polarization vs electric field (*P*–*E*) hysteresis loop, and Raman spectroscopy. **Figure 2**a shows SEM images of top PZT surfaces annealed at three different temperatures to obtain statistical data of the grain-size distributions. The average grain sizes of the AD PZT were calculated from the top view images as 61.6, 84.5, and 125.4 nm at corresponding annealing temperatures of 700, 800, and 900 °C, respectively. Since the critical grain size for a perovskite PZT material is typically less than 100 nm, dense and crack-free AD PZT films above the critical grain size would have excellent properties similar to those of bulk ceramics owing to minimized negative interference between ferroelectric domains and grain boundaries.[40] Figure 2b presents the XRD measurements of flexible PZT films annealed at 700, 800, and 900 °C, which show that the PZT samples were well crystallized with pure perovskite peaks. The intensity of the perovskite PZT peaks was enhanced by higher annealing temperature, and the full width at half maximum (FWHM) of the (110) peak gradually decreased as the temperature increased.[41] From the Scherrer equation $D = 0.94\lambda/\beta\cos\theta$ (where D is the average crystallite size, λ is the X-ray wavelength, β is the line broadening at FWHM, and θ is the Bragg angle), the smaller FWHM of the PZT peak at the higher annealing temperature from the XRD verified the grain growth of the AD PZT film with elevated temperature from 700 to 900 °C.[42] Figure 2c depicts the *P*–*E* hysteresis loops of PZT films with different annealing temperatures at a maximum electric field of 70 kV cm^{-1}. From these loops, the remnant and saturated polarization values of the AD PZT samples increased as the annealing temperature increased. The grain size of PZT ceramic films with the same film thickness of 7 µm is solely responsible for the different remnant and saturated polarization values.[43] When the grain size of PZT decreases below a critical size, the strong coupling between the ferroelectric domains and the grain boundaries increases the repulsive force of the neighboring domains, which thus results in a reduction of remnant and saturated polarization.[44] The low-domain wall mobility at smaller grain size reduces the piezoelectric constants of PZT ceramics, causing a performance drop of piezoelectric harvesters.[39] Raman spectroscopy was

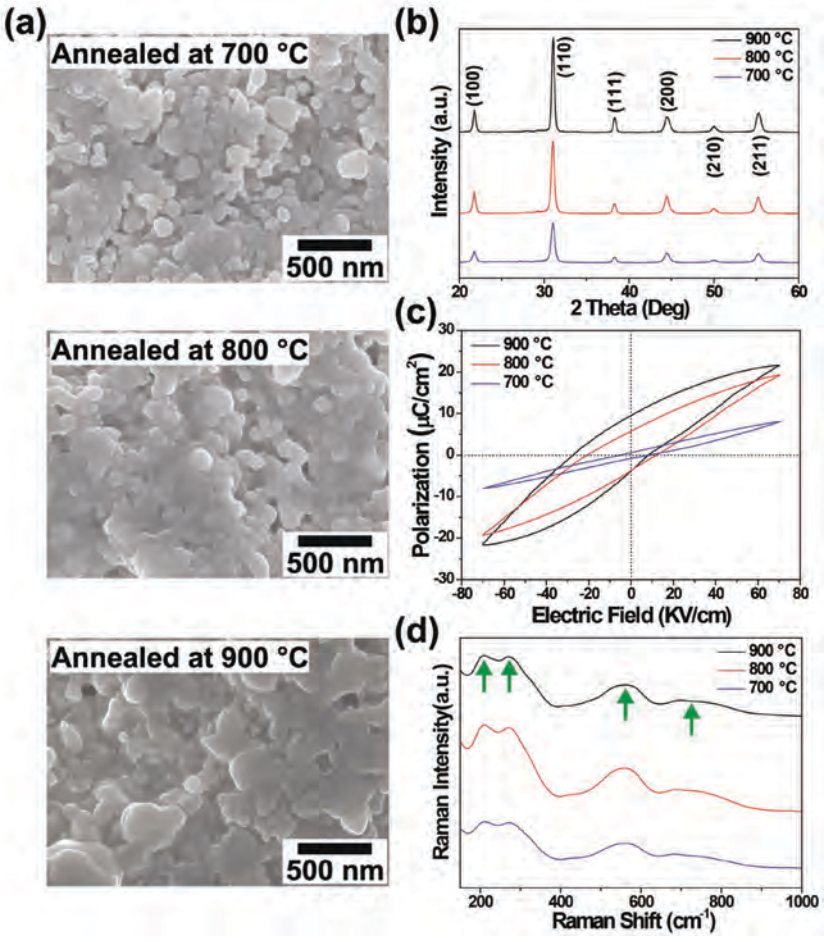

Figure 2. a) Top-view SEM images of AD PZT thick films deposited on sapphire substrates and annealed at temperatures of 700, 800, and 900 °C. b) XRD patterns of AD PZT thick films annealed at three different temperatures. c) Polarization–electric (*P*–*E*) hysteresis loops of the flexible ferroelectric PZT films as a function of annealing temperature at room temperature. d) Raman spectra of the high-temperature-annealed AD PZT films transferred onto PET substrates.

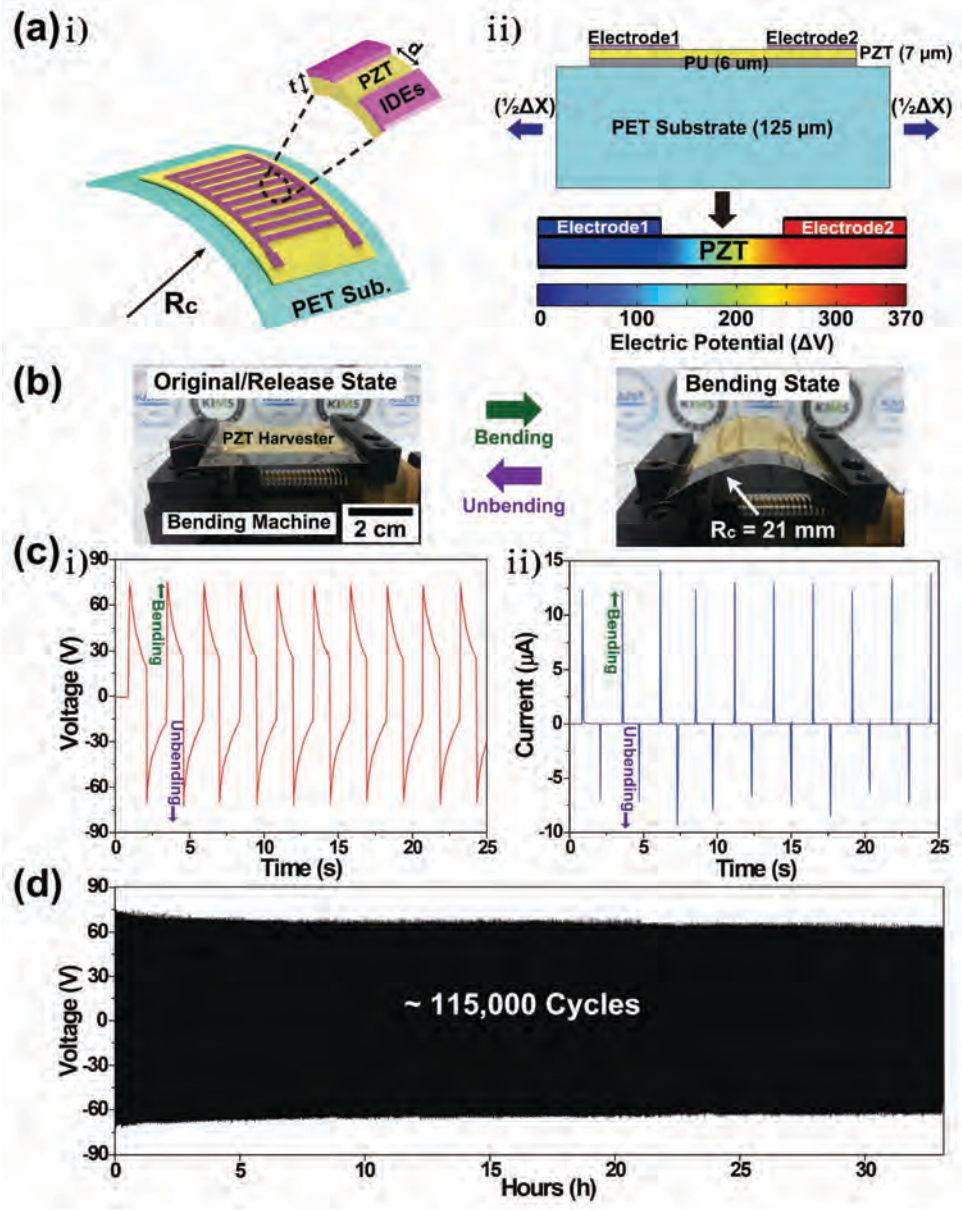

Figure 3. a) A simulation model of (i) an IDE-type flexible PZT-film energy harvester and (ii) calculated piezopotential distribution inside the AD PZT thick film. b) A photograph of the flexible AD PZT harvesting device in bent and unbent states for energy generation. c) The open-circuit voltage (i) and short-circuit current values (ii) from the flexible PZT energy harvester during periodic bending and unbending motions. d) The result of a bending durability test over around 115,000 cycles to verify the mechanical stability of the flexible harvester.

carried out, as shown in Figure 2d, to examine the phases of the AD PZT films annealed at the three different aforementioned temperatures by using a 514.5 nm Ar^+ ion laser. All AD PZT samples have similar shapes of Raman spectra peaks located at 210, 270, 560, and 735 cm^{-1}, which correspond to the E(2TO), E+B_1, A_1(3TO), and E(3LO) modes, respectively, in good agreement with the typical rhombohedral perovskite phase close to the morphotropic phase boundary (MPB).[45]

To predict the output performance of the flexible AD PZT harvester, we simulated theoretically the piezoelectric potential produced inside the PZT film using a finite-element analysis (FEA). **Figure 3**a-i and a-ii show the device model and calculated piezopotential distribution of the piezoelectric PZT layer with lateral IDE. The calculation was performed with a simplified simulation model composed of top metal electrodes with an intergap of 100 μm, a PZT film (thickness of 7 μm, a piezoelectric charge coefficient of d_{33} = 406 pC N^{-1}, dielectric constant of K^T = 1100, Young's modulus of E = 60 GPa, and mass density of 7800 kg m^{-3}), and an adhesive PU layer (thickness of 6 μm) on a PET substrate (thickness of 125 μm) at a bending radius of 21 mm (corresponding to applied tensile strain of 0.3% on the PET). The PET film is elongated in the parallel direction for a total displacement (ΔX) of 150 μm from the relationship $S = \Delta X/X_o$ (where S is the tensile strain

and X_0 is the initial width). The 7 μm thick AD PZT film on a flexible substrates shows a maximum piezopotential difference (ΔV) of 370 V between the neighboring lateral electrodes upon the strained force, as illustrated in Figure 3a-ii. The calculation result indicates that the flexible PZT harvesting device can generate a high output voltage across the IDE intergap. The IDE flexible energy harvesters with an interelectrode gap of a hundred micrometers could provide a higher output voltage than metal–insulator–metal (MIM) harvesters with the same film thickness of 7 μm, as the piezoelectric potential increases proportionally more with greater distance between the electrodes (see Figure S3 in Supporting Information).[46]

The output performance of the flexible AD PZT harvester was characterized by a linear motor which made repetitive bending and unbending motions (Figure 3b) with a curvature radius of 21 mm, a tensile strain of 0.3%, a strain rate of 2.2%·s^{-1}, and a frequency of 0.4 Hz; the calculated effective tensile strain of PZT active layer in the multilayered energy harvester was 0.16% (see Supporting Information), which was below the fracture strain of PZT.[47,48] The periodic bending deformations of the harvesting devices generated electric output signals due to the piezoelectric potential inside the PZT film on the plastic substrate. Figures 3c-i and c-ii present the characterized electric output values from the flexible piezoelectric harvester. The generated open-circuit voltage and the short-circuit current from the repeated bending motions of the piezoelectric harvester were 75 V and 14 μA, respectively. Furthermore, the maximum output signals of 200 V and 35 μA (corresponding output current density of 5.6 μA cm^{-2}) were obtained from a slight bending by human fingers, which immediately induced a high strain rate in the device (see Figure S4 in Supporting Information). These output values were higher than those of a previously reported flexible single-crystalline PMN-PZT energy harvester using top lateral IDEs, which generated an open-circuit voltage of 100 V and a short-circuit current of 20 μA (corresponding output current density of 6.1 μA cm^{-2}) by a similar hand motion. The notable output performance of the flexible harvester is achieved by the enhanced piezoelectric properties from the high-quality (dense and crack-free) PZT thick film and the high temperature annealing at 900 °C. The piezoelectric properties of single crystals are seriously degraded by decreased film thickness below several tens of micrometers, while those of polycrystalline materials are not related to film thickness.[49,50] Therefore, polycrystalline piezoelectric films below 10 μm are advantageous in terms of the output performance of flexible energy harvester compared to similar-thickness piezoelectric single crystals. The output voltage and current signals of a flexible harvester annealed at 900 °C were five times and 7.5 times higher than a sample annealed at 700 °C, as shown in Figure S5 (see Supporting Information), which indicates that the performance is directly proportional to the film quality. The mechanical durability of the flexible energy harvester throughout a considerable number of bending cycles is shown in Figure 3d. The stable output voltage values were maintained without significant variation for around 115,000 bending iterations at an induced strain of 0.3% on the PET substrate. The exceptional working endurance of the flexible energy harvester in the harsh repetitive conditions is credited to the mechanical robustness of the flexible AD PZT film.[51]

Figure 4a shows the recorded voltage and current peaks as a function of various external resistances ranging from 120 to 440 MΩ to investigate the instantaneous output power of the flexible PZT harvester bent in the bending stage. The voltage output values steadily increased and saturated from a low resistance to a high resistance, while the current signals gradually decreased and saturated as the load resistance increased. The instantaneous output power of the piezoelectric harvesting device was calculated by multiplying the voltage and current output values obtained at a specific external resistance.[21] As a result, a maximum instantaneous power of 0.2 mW (46 V × 4.5 μA) was generated at a resistance of 10 MΩ, as shown in the inset of Figure 4a. To exploit the flexible AD PZT harvester as a power source of a WSN, the electricity from the self-powered harvester must be stored in storage elements such as supercapacitors and batteries.[52] The piezoelectric energy harvesters generate an AC-type signal that should be converted into DC output by a full wave bridge rectification circuit to match normal DC electronic systems.[53] Figure 4b shows that a rectified voltage of 70 V was measured from the bending motions of the flexible harvester. This output energy is sufficiently high to directly charge a supercapacitor (22 mF capacity) and operate low-power-consumption consumer electronics or WSN devices. Figure 4c presents the charging curve of a supercapacitor from 0 to 2 V by using the flexible PZT energy harvester with an induced strain of 0.3% on PET, a strain rate of 2.2%·s^{-1}, and a frequency of 1.7 Hz, and the inset shows the circuit schematics of energy storage. Even though energy storage with a supercapacitor by flexible harvesters is difficult due to energy loss from impedance mismatch, a high-output AD PZT generator could overcome the power loss and charge a supercapacitor.[54] Figure 4d shows that 208 blue LEDs were turned on by the electric output of harvested energy by human hands (see Video S1 in Supporting Information).

To demonstrate a self-powered wireless sensor node, we fabricated a total electronic system including flexible PZT energy harvesters, a bridge rectifier, a storage capacitor, and a commercially available wireless temperature-sensor node (eZ430-RF2500T, Texas Instruments) as presented in **Figure 5**a. Under periodic bending motions, the electric AC signal was generated from the two piezoelectric harvesters connected in parallel and simultaneously converted via the rectifying circuit into DC output to charge a 1 mF capacitor. Finally, the RF temperature sensor node received the electric power from the charged capacitor to measure ambient temperature and then wirelessly transmit the information to a 2.4 GHz RF receiver linked to a computer, where the temperature data can be displayed on a monitor (see Video S2 in Supporting Information).[55] As depicted in Figure 5b, the electric energy from the piezoelectric harvesting devices can be used to charge the capacitor from 0 to 4.3 V within around 45 min, and discharged in sequence to operate the wireless temperature sensor node 18 times at intervals of about 45 s. The capacitor voltage was immediately dropped down to about 3 V roughly at t = 45 min as the sensor node network was initialized for operation, setting the supply voltage (V_{CC}) to its typical value. There was another dramatic

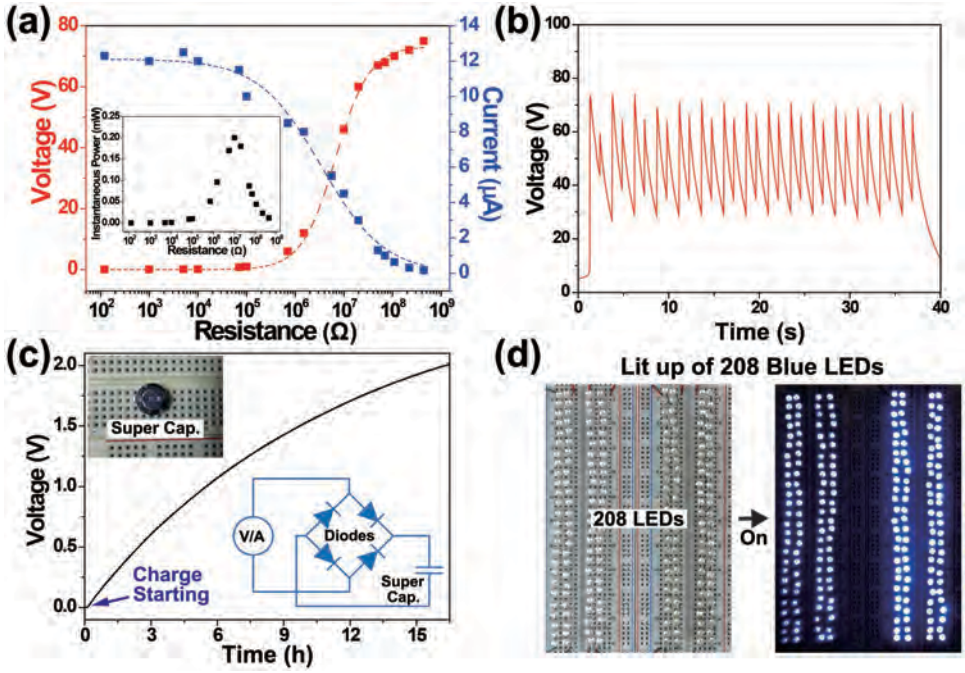

Figure 4. a) The measured output voltage (red dots) and output current (blue dots) signals under different load resistance varying from 120 Ω to 440 MΩ. The inset shows the instantaneous output power calculated from the generated voltage and current values. b) The open-circuit voltage of the flexible piezoelectric harvesting device rectified by a full-wave-bridge rectifier. c) The charging curve of a supercapacitor (capacity 22 mF) using the AD PZT energy harvester. The inset shows a schematic circuit diagram of an energy-harvesting and storage system composed of a flexible harvester, rectifier, and supercapacitor. d) A photograph of 208 blue LEDs lighting up when the flexible energy-harvesting device was bent by human hand.

voltage decay observed after the completion of entire temperature sensing and wireless transmission cycles. Here, we suspect that remaining charges in the storage capacitor leaked out as the capacitor voltage was reduced below the minimum value required for the sensor-node operation. The inset of Figure 5b shows a photograph of the RF sensor module and the capacitor electrically connected on a bread board. The wireless sensor node incorporates an ultralow power microcontroller unit with an internal temperature sensor (MSP430F2274, Texas Instruments), a 2.4 GHz RF transceiver chip (CS2500, Texas Instruments), and a chip antenna, which requires an aggregate input power above 20 mW for 20 ms (corresponding total consumption energy above 400 μJ).[56] Here, 260 strain cycles of the flexible piezoelectric harvesters were required for operation of each wireless sensing device. We anticipate that the operating efficiency of our self-powered WSN system can be significantly improved, even to the level of real-time monitoring, by adopting advanced conversion circuits or ultralow power-sensor node design.[20,54] To verify the proper operation of wireless communication, we characterized the voltage output from one of the external digital input/output (I/O) pins available on both the transmitter and receiver target boards. The measured pin was specifically chosen to test whether the harvester supplied sufficient power to drive the wireless sensor module. The voltage output of this I/O pin on each target board is shown in Figure 5c. In the transmitter, the voltage output was dropped from 2.7 V to –0.4 V and remained low for 20 ms, which indicates complete operation of temperature sensing, signal controlling/modulation, analog-to-digital conversion, bandpass filtering, and RF signal transmission (a detailed description of the procedure by the microcontroller and RF transceiver can be found in the manufacturer's datasheets).[56] In the receiver, the output voltage instantaneously dropped from 3 V to –0.5 V, which was in phase with the voltage output edge of the transmitter. The simultaneous voltage output drops show that both transceivers mutually transmit and receive the RF signal, which confirms wireless communication between the two boards. Figure 5d presents the variation of room temperature vs time during 800 s of telecommunication from the RF temperature sensor, and the inset shows the ambient temperature measured by a digital thermometer, which was used to verify our sensing accuracy.

In summary, a piezoelectric AD PZT film prepared with single-step deposition and postannealing was successfully utilized to fabricate a high-performance flexible piezoelectric harvester via a fast, simple, and cost-effective method. The high-temperature-annealed AD PZT thick film on a rigid sapphire substrate was transferred onto a flexible substrate by the ILLO process. The flexible PZT harvester can convert a maximum output voltage of 200 V and a current signal of 35 μA from biomechanical bending motions; these values are comparable to those of a similar IDE-type flexible single-crystal energy harvester. Moreover, our AD PZT film is advantageous in terms of production cost and process time to realize the mass production of flexible harvesting devices compared to piezoelectric single crystals that require high-cost and time-consuming process.[21] The high-output performance of the energy harvester originates from the large grain growth of the PZT ceramic film under the high temperature annealing process at 900 °C, which leads to outstanding piezoelectric harvesting properties with

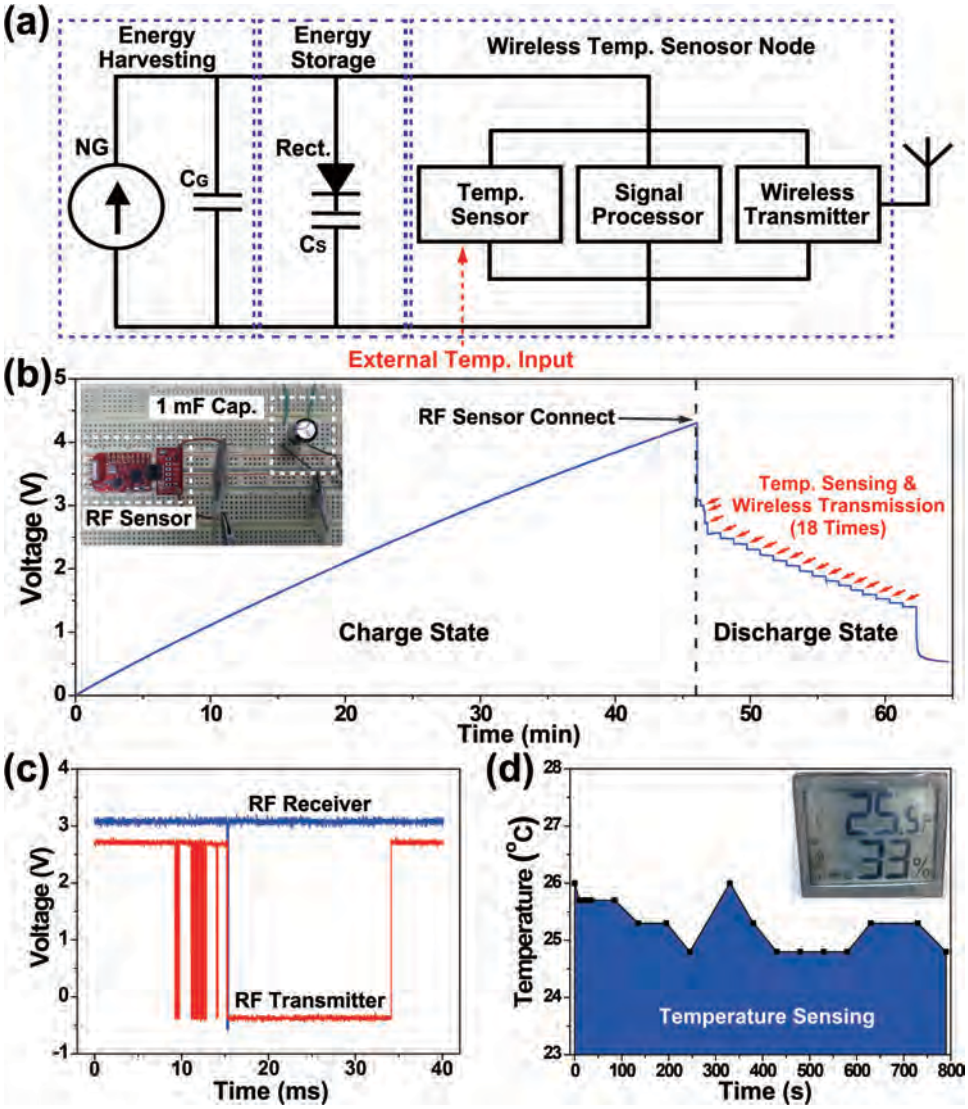

Figure 5. a) A schematic circuit diagram of the self-powered wireless temperature sensor-node system. b) Charging and discharging curve of a capacitor (capacity 1 mF) for energy storage by the flexible PZT energy harvester and subsequent operation of RF temperature sensor node. c) Measured digital voltage output from I/O pins of the RF transmitter module (in red) and the RF receiver module (in blue). d) The recorded temperature transmitted from the wireless sensor node system over 800 s. The inset shows a digital thermometer that presents ambient room temperature.

robust endurance for up to around 115,000 bending cycles on a flexible substrate. By storing electrical power from the flexible harvester, we demonstrated a self-powered wireless temperature sensor node system consisting of flexible AD harvesters, rectifying/storage elements, and an RF sensing device. The generated electricity was used to charge a capacitor up to 4.3 V within about 45 min and operate a wireless sensor node 18 times, which included measurement of ambient temperature and wireless transmission. This verifies the feasibility of our flexible AD piezoelectric energy harvester for operating a self-powered WSN or IoT, with specific applications such as structural/environmental monitoring, human healthcare, and military/personal electronic devices. We are currently integrating the flexible AD harvester with a high-efficiency conversion circuit and a customized ultralow-power wireless sensor module to achieve the real-time operation of self-powered WSN.[20]

Experimental Section

Aerosol Deposition (AD) of PZT Film: Before AD deposition process, commercially available PZT granules (for properties see Table S1 in Supporting Information) were pre-heat treated at 400 °C for 5 h to remove moisture and organic substances, and the sapphire substrate was rinsed with acetone, ethanol, and deionized water, to remove some ionic contaminants. The heat-treated granules were mixed with a carrier gas (medical grade dried air with flow rate of 240 L min^{-1}) using an in-house-designed constant-rate granule-feeding system, and then ejected through a nozzle with a rectangular orifice (1 × 400 mm) to be sprayed onto a moving substrate in a vacuum chamber at about 5 Torr. To obtain a desired thickness of the film, the number of substrate scans was controlled.

Fabrication of Flexible AD PZT Energy Harvester: A high-quality piezoelectric PZT thick film (thickness in 7 μm) was formed on a 2-inch sapphire wafer (430 μm thick, Hi-solar Co.) by the AD process. The deposition time was around 5 min to fabricate a 7 μm-thick PZT film. The PZT film was subsequently annealed at above 700 °C for 1 h in a

furnace to enhance the crystallization of PZT material. A PET film rinsed with acetone, ethanol, and deionized water was bonded to the PZT thick film by using a UV-curable PU adhesive (NOA 73, Norland Products Inc.). The PZT/PET layer was attached to a carrier glass substrate for maintaining flatness of device to avoid PZT cracking caused by abrupt deformations during harsh device handling motions during the fabrication process. To delaminate the PZT film from the mother substrate, an XeCl excimer laser (energy density of ca. 420 mJ cm^{-2} and pulse frequency of 10 Hz) was used to irradiate the reverse side of the sapphire wafer. The scan speed and spot size of the laser beam on the sample were 3.7 mm s^{-1} and 625 μm^2, respectively. Afterward, a Cr (5 nm)/Au (100 nm) electrode layer was deposited onto the flexible PZT film by using an RF sputtering system and then defined by using a photolithography technique. The SU8 (thickness of 5 μm, MicroChem Co.) passivation layer was directly spin-coated onto the surface of the flexible energy harvester to avoid physical damage during the polling process and device bending. Finally, Cu wires were attached to the AD PZT harvester by using a silver conductive paste.

Measurement of Electrical Characteristics: The output performance of flexible AD PZT harvester was characterized by using a custom-designed bending stage and a Keithley 2612A source-meter with periodic bending deformation of the harvesting device.

Supporting Information

Supporting Information is available from the Wiley Online Library or from the author.

Acknowledgements

G.-T.H. and V.A. contributed equally to this work. Work at KAIST was supported by Korea-Sweden research cooperation program (grant code: 2014R1A2A1A12067558), Global Frontier R&D Program on Center for Integrated Smart Sensors (grant No. CISS-2012M3A6A6054193) through the National Research Foundation of Korea (NRF) funded by the Ministry of Science, ICT and future Planning. Work at KIMS was supported by KIMS' internal R&D program (Project. No. PNK4661).

Received: February 2, 2016
Revised: February 25, 2016
Published online:

[1] A. Nechibvute, A. Chawanda, P. Luhanga, *Smart Mater. Res.* **2012**, *2012*, 853481.
[2] Z. L. Wang, *Adv. Mater.* **2012**, *24*, 280.
[3] H. L. Zhang, Y. Yang, Y. J. Su, J. Chen, C. G. Hu, Z. K. Wu, Y. Liu, C. P. Wong, Y. Bando, Z. L. Wang, *Nano Energy* **2013**, *2*, 693.
[4] J. Ryu, J. E. Kang, Y. Zhou, S. Y. Choi, W. H. Yoon, D. S. Park, J. J. Choi, B. D. Hahn, C. W. Ahn, J. W. Kim, Y. D. Kim, S. Priya, S. Y. Lee, S. Jeong, D. Y. Jeong, *Energy Environ. Sci.* **2015**, *8*, 2402.
[5] Z. L. Wang, J. H. Song, *Science* **2006**, *312*, 242.
[6] K. I. Park, S. Xu, Y. Liu, G. T. Hwang, S. J. L. Kang, Z. L. Wang, K. J. Lee, *Nano Lett.* **2010**, *10*, 4939.
[7] S. H. Lee, C. K. Jeong, G. T. Hwang, K. J. Lee, *Nano Energy* **2015**, *14*, 111.
[8] X. D. Wang, *Nano Energy* **2012**, *1*, 13.
[9] Y. F. Hu, Y. Zhang, C. Xu, G. A. Zhu, Z. L. Wang, *Nano Lett.* **2010**, *10*, 5025.
[10] Y. Qi, M. C. McAlpine, *Energy Environ. Sci.* **2010**, *3*, 1275.
[11] X. D. Wang, J. H. Song, J. Liu, Z. L. Wang, *Science* **2007**, *316*, 102.
[12] K. I. Park, M. Lee, Y. Liu, S. Moon, G. T. Hwang, G. Zhu, J. E. Kim, S. O. Kim, D. K. Kim, Z. L. Wang, K. J. Lee, *Adv. Mater.* **2012**, *24*, 2999.
[13] K. I. Park, C. K. Jeong, J. Ryu, G. T. Hwang, K. J. Lee, *Adv. Energy Mater.* **2013**, *3*, 1539.
[14] M. Y. Choi, D. Choi, M. J. Jin, I. Kim, S. H. Kim, J. Y. Choi, S. Y. Lee, J. M. Kim, S. W. Kim, *Adv. Mater.* **2009**, *21*, 2185.
[15] J. Kwon, W. Seung, B. K. Sharma, S. W. Kim, J. H. Ahn, *Energy Environ. Sci.* **2012**, *5*, 8970.
[16] C. Dagdeviren, B. D. Yang, Y. W. Su, P. L. Tran, P. Joe, E. Anderson, J. Xia, V. Doraiswamy, B. Dehdashti, X. Feng, B. W. Lu, R. Poston, Z. Khalpey, R. Ghaffari, Y. G. Huang, M. J. Slepian, J. A. Rogers, *Proc. Natl. Acad. Sci. USA* **2014**, *111*, 1927.
[17] C. Dagdeviren, S. W. Hwang, Y. W. Su, S. Kim, H. Y. Cheng, O. Gur, R. Haney, F. G. Omenetto, Y. G. Huang, J. A. Rogers, *Small* **2013**, *9*, 3398.
[18] Y. F. Hu, Y. Zhang, C. Xu, L. Lin, R. L. Snyder, Z. L. Wang, *Nano Lett.* **2011**, *11*, 2572.
[19] G. T. Hwang, H. Park, J. H. Lee, S. Oh, K. I. Park, M. Byun, H. Park, G. Ahn, C. K. Jeong, K. No, H. Kwon, S. G. Lee, B. Joung, K. J. Lee, *Adv. Mater.* **2014**, *26*, 4880.
[20] G. T. Hwang, J. Yang, S. H. Yang, H. Y. Lee, M. Lee, D. Y. Park, J. H. Han, S. J. Lee, C. K. Jeong, J. Kim, K. I. Park, K. J. Lee, *Adv. Energy Mater.* **2015**, *5*, 1500051.
[21] G. T. Hwang, Y. Kim, J. H. Lee, S. Oh, C. K. Jeong, D. Y. Park, J. Ryu, H. Kwon, S. G. Lee, B. Joung, D. Kim, K. J. Lee, *Energy Environ. Sci.* **2015**, *8*, 2677.
[22] G. T. Hwang, M. Byun, C. K. Jeong, K. J. Lee, *Adv. Healthcare Mater.* **2015**, *4*, 646.
[23] S. E. E. Park, W. Hackenberger, *Curr. Opin. Solid State Mater.* **2002**, *6*, 11.
[24] H. Kozuka, M. Kajimura, *J. Am. Ceram. Soc.* **2000**, *83*, 1056.
[25] J. Akedo, M. Lebedev, *Jpn. J. Appl. Phys.* **1999**, *38*, 5397.
[26] G. Han, J. Ryu, W. H. Yoon, J. J. Choi, B. D. Hahn, D. S. Park, *J. Am. Ceram. Soc.* **2011**, *94*, 1509.
[27] Q. F. Zhou, S. T. Lau, D. W. Wu, K. Shung, *Prog. Mater. Sci.* **2011**, *56*, 139.
[28] J. Ryu, S. Priya, C. S. Park, K. Y. Kim, J. J. Choi, B. D. Hahn, W. H. Yoon, B. K. Lee, D. S. Park, C. Park, *J. Appl. Phys.* **2009**, *106*, 024108.
[29] S. Kim, J. H. Son, S. H. Lee, B. K. You, K. I. Park, H. K. Lee, M. Byun, K. J. Lee, *Adv. Mater.* **2014**, *26*, 7480.
[30] D. H. Kim, J. Viventi, J. J. Amsden, J. L. Xiao, L. Vigeland, Y. S. Kim, J. A. Blanco, B. Panilaitis, E. S. Frechette, D. Contreras, D. L. Kaplan, F. G. Omenetto, Y. G. Huang, K. C. Hwang, M. R. Zakin, B. Litt, J. A. Rogers, *Nat. Mater.* **2010**, *9*, 511.
[31] I. R. Henderson, *Piezoelectric Ceramics: Principles and Applications APC International*, APC International, Ltd., Pennsylvania, USA **2006**.
[32] G. T. Hwang, D. Im, S. E. Lee, J. Lee, M. Koo, S. Y. Park, S. Kim, K. Yang, S. J. Kim, K. Lee, K. J. Lee, *ACS Nano* **2013**, *7*, 4545.
[33] Y. G. Sun, J. A. Rogers, *Adv. Mater.* **2007**, *19*, 1897.
[34] G. Han, J. Ryu, W. H. Yoon, J. J. Choi, B. D. Hahn, J. W. Kim, D. S. Park, C. W. Ahn, S. Priya, D. Y. Jeong, *J. Appl. Phys.* **2011**, *110*, 124101.
[35] J. V. Biggers, S. Venkataramani, *Mater. Res. Bull.* **1978**, *13*, 717.
[36] K. I. Park, J. H. Son, G. T. Hwang, C. K. Jeong, J. Ryu, M. Koo, I. Choi, S. H. Lee, M. Byun, Z. L. Wang, K. J. Lee, *Adv. Mater.* **2014**, *26*, 2514.
[37] Y. H. Do, M. G. Kang, J. S. Kim, C. Y. Kang, S. J. Yoon, *Sens. Actuators A* **2012**, *184*, 124.
[38] C. H. Lee, S. J. Kim, Y. Oh, M. Y. Kim, Y. J. Yoon, H. S. Lee, *J. Appl. Phys.* **2010**, *108*, 102814.
[39] C. A. Randall, N. Kim, J. P. Kucera, W. W. Cao, T. R. Shrout, *J. Am. Ceram. Soc.* **1998**, *81*, 677.

[40] K. Uchino, E. Sadanaga, K. Oonishi, T. Morohashi, H. Yamamura, in *Ceramic Dielectrics: Composition, Processing and Properties. Proc. Symp. on Ceramic Dielectrics*, Indianapolis **1989**, p. 107.
[41] Y. K. Fu, S. Y. Gong, X. F. Liu, G. Xu, Z. H. Ren, X. Li, G. R. Han, *J. Mater. Chem. C* **2015**, *3*, 382.
[42] A. L. Patterson, *Phys. Rev.* **1939**, *56*, 978.
[43] T. A. Kamel, G. de With, *J. Eur. Ceram. Soc.* **2008**, *28*, 851.
[44] S. H. Hu, G. J. Hu, X. J. Meng, G. S. Wang, J. L. Sun, S. L. Guo, J. H. Chu, N. Dai, *J. Cryst. Growth* **2004**, *260*, 109.
[45] A. G. Souza, K. C. V. Lima, A. P. Ayala, I. Guedes, P. T. C. Freire, F. E. A. Melo, J. Mendes, E. B. Araujo, J. A. Eiras, *Phys. Rev. B* **2002**, *66*, 132107.
[46] Y. B. Jeon, R. Sood, J. H. Jeong, S. G. Kim, *Sens. Actuators A* **2005**, *122*, 16.
[47] X. Feng, B. D. Yang, Y. M. Liu, Y. Wang, C. Dagdeviren, Z. J. Liu, A. Carlson, J. Y. Li, Y. G. Huang, J. A. Rogers, *ACS Nano* **2011**, *5*, 3326.
[48] S. I. Park, A. P. Le, J. A. Wu, Y. G. Huang, X. L. Li, J. A. Rogers, *Adv. Mater.* **2010**, *22*, 3062.
[49] H. Lee, S. J. Zhang, J. Luo, F. Li, T. R. Shrout, *Adv. Funct. Mater.* **2010**, *20*, 3154.
[50] D. Lin, H. J. Lee, Shujun Zhanga, F. Lia, Z. Li, Z. Xu, T. R. Shrouta, *Scr. Mater.* **2011**, *68*, 1149.
[51] C. K. Jeong, K. I. Park, J. H. Son, G. T. Hwang, S. H. Lee, D. Y. Park, H. E. Lee, H. K. Lee, M. Byun, K. J. Lee, *Energy Environ. Sci.* **2014**, *7*, 4035.
[52] C. K. Jeong, K. I. Park, J. Ryu, G. T. Hwang, K. J. Lee, *Adv. Funct. Mater.* **2014**, *24*, 2620.
[53] C. K. Jeong, J. Lee, S. Han, J. Ryu, G. T. Hwang, D. Y. Park, J. H. Park, S. S. Lee, M. Byun, S. H. Ko, K. J. Lee, *Adv. Mater.* **2015**, *27*, 2866.
[54] J. Yang, S. Lee, J. Kim, *Electron. Lett.* **2014**, *50*, 629.
[55] M. Johnson, M. Healy, P. v. d. Ven, M. J. Hayes, J. Nelson, T. Newe, E. Lewis, in *Sensors, 2009 IEEE*, Christchurch **2009**, p. 1439.
[56] Texas Instruments, eZ430-RF2500 Development Tool, http://www.ti.com/tool/ez430-rf2500 (accessed: June 2015).